https://dx.doi.org/10.1016/j.seta.2022.101993

A new battery thermal management system employing the mini-channel cold plate with pin fins

Zengjia Guo[1], Qidong Xu[1], Siyuan Zhao[1], Shuo Zhai[1], Tianshou Zhao[2,*], Meng Ni[1,*]

[1] Department of Building and Real Estate, Research Institute for Sustainable Urban Development (RISUD) and Research Institute for Smart Energy (RISE), The Hong Kong Polytechnic University, Hung Hom, Kowloon, Hong Kong, China

[2] Department of Mechanical and Aerospace Engineering, Hong Kong University of Science and Technology, Hong Kong, China

* Corresponding authors: metzhao@ust.hk (T.S. Zhao); meng.ni@polyu.edu.hk (M. Ni)

Abstract: Batteries are critical for energy storage and electrical vehicles. In this study, a new battery thermal management system (BTMS) is proposed by employing a mini-channel cold plate with pin fins. The performance of BTMS is evaluated by a 3D numerical model. The heat transfer characteristics, pressure loss and flow structure in the BTMS are analyzed, and the performance of BTMS is evaluated using efficiency index (*EI*) which considers both heat transfer performance and pressure loss. It is found that pin fins can improve the heat transfer performance of BTMS with acceptable pressure loss. Therefore, the *EI* of BTMS with pin fins is always greater than 1. It is also found that the BTMS with 4 x 3 staggered arranged pin fins outperforms that with the 3 x 4 staggered arrangement and 4 x 4 inline arrangement in *EI*. Although the horizontally arranged pin fins greatly enhances heat transfer, the pressure loss by the pin fins is also significant. As a result, *EI* of BTMS with vertically arranged pin fins was 4.54% higher than that of BTMS with horizontally arranged pin fins.

Keywords:

Battery thermal management system; Pin fins; Mini-channel cold plate; Heat transfer improvement; Efficiency index.

Nomenclature

ρ	Density[kg/m^3]
c_p	Specific heat capacity[J/kg•K]
λ	Heat conductivity coefficient[W//m•K]
Q_g	Total generated heat[W]
Q_r	Reaction heat
Q_j	Ohmic heat
Q_p	Polarization heat
I	Discharge current
E_{oc}	Open circuit voltage
R_e	Pure resistance of battery
R_p	Polarization resistance
R_t	Total resistance
$\vec{v}$	Velocity vector
P	Pressure [Pa]
D_h	Hydraulic diameter
V_t	Volume of mini-channels without pin fins
V_p	Volume of pin fins
A_f	Effective heat transfer area
Nu	Nusselt number
q	Heat flux
f	Friction factor
ΔP	Pressure loss between the inlet and outlet
u	Average velocity
L	Length of mini-channel

Subscripts

b	Battery
c	Cooling medium
m	Mini-channel cold plate
oc	Open circuit
r	Reaction
j	Joule
p	Polarization

Acronyms

BTMS	Battery thermal management system
EI	Efficiency index
UDF	User defined function
HEV	Hybrid electric vehicle
EV	Electric vehicle
PCM	Phase change material
3D	Three dimensions
EC	Ethylene carbonate
DMC	Dimethyl carbonate
EMC	Ethyl methyl carbonate

1 Introduction

Electric vehicles (EVs) and hybrid electric vehicles (HEVs) are receiving more and more attention in recent years because of their zero or low pollution on the road [1]. Lithium-ion (Li-ion) batteries are preferred in both EVs and HEVs due to their high energy density, low self-discharge rate, and long life cycle [2]. Significant amount of heat can be generated from Li-ion batteries during charging/discharging process. However, the performance, lifetime, reliability, and safety of Li-ion batteries can be easily affected by the temperature. Under some extreme conditions, permanent capacity degradation and thermal runaway can take place [3]. In addition, the temperature distribution of single battery and battery pack can be non-uniform, which in turn can affect the battery performance and lifetime [4]. Yan [5] and Pesaran [6] pointed out that the optimal working temperature of Li-ion battery is between 15℃ and 40℃, and maximum temperature difference should be below 5℃. Therefore, an effective battery thermal management system (BTMS) is essential for the efficient, stable, and safe operation of the battery pack.

Depending on the different types of working mediums used, the BTMS can be divided into air cooling, liquid cooling, and phase change materials (PCM) cooling. The performance of air cooling BTMS is directly influenced by the airflow pattern and battery layout. Na [7] proposed a reversely layered airflow for comparison with the unidirectional airflow. The novel structure achieved lower battery maximum temperature and more uniform temperature distribution. Saw [8] numerically investigated air cooling BTMS and reported higher heat transfer with negligibly increased pressure loss at a higher mass flow rate. Wang [9] and Yang [10] demonstrated that appropriate battery arrangement played an important role in designing efficient BTMS. Hallaj [11] pioneered the application of PCM to the BTMS as a novel and efficient cooling method. Rao [12] proposed several essential requirements for the selection of PCM in the BTMS. Through the extensive efforts of researchers, paraffin wax and paraffin mixtures are widely used in BTMS with PCM [13-15]. In addition, BTMS with heat pipe also achieved good performance. Yong [16] optimized the BTMS with heat pipe for fast discharging and charging to ensure the cooling performance. Zhang [17] proposed a BTMS with heat pipes which are combined with fins, improving the heat transfer performance and temperature uniformity. Wang [18] proposed a BTMS with micro heat pipe array, achieving good performance in cooling and heating battery pack.

Due to the high convective heat transfer coefficient and excellent compactness, liquid cooling BTMS has become a very attractive option. Water, the mixture of water and glycol [19], mineral/silicon oil [20], nanofluid [21, 22], and liquid metal [23] have been used as the coolant to directly cool the battery pack. BTMS with the mini-channels cold plate received more attention because of the excellent cooling performance and lower risk of leakage and corrosion. Panchal [24], Jarrett [25], and Karimi [26] respectively investigated serpentine type, U-turn type, and Z-turn type flow path cold plates. They found that there are more contact areas for coolant in these flow paths to absorb heat, resulting in better heat transfer performance and temperature uniformity compared to the linear-type path. Yuan [27] conducted the investigation to optimize the cold plate flow path by both experiments and numerical simulations. The cold plate with one inlet and one outlet showed poor heat transfer performance because of the too-long flow path. For comparison, the cold plate with multi mini channels showed better heat transfer performance. Huo [28] explored the effect of mini-channels number, flow direction, and inlet flow rate on heat transfer performance. The maximum temperature was found to decrease with increasing channel number and inlet flow rate, and the effect of flow direction decreased with increasing inlet flow rate. Qian [29] numerically investigated the heat transfer performance and pressure loss of BTMS with the mini-channels cold plate. It was pointed out that there is always an optimum inlet flow rate for BTMS, considering both maximum temperature and pressure loss. The other geometric parameters such as the channel diameter

[30] and shape [31] have also been investigated to achieve the balance between the maximum temperature and pressure loss.

However, for liquid cooling BTMS, the thickness of the thermal boundary layer will gradually increase with increasing liquid flow rate. This phenomenon will lead to the deterioration in convective heat transfer performance, leading to higher maximum temperature and uneven temperature distribution [32]. Therefore, new BTMS designs that can improve heat transfer and reduce temperature gradients are needed for effective BTMS. Jin [33] proposed an oblique fin to redevelop the boundary layer periodically, achieving lower temperature and more uniform temperature distribution with the acceptable pressure loss. Mohammed [34] proposed a dual-purpose cold plate for the normal operation and thermal runaway by adding staggered pins. Nur [35] investigated the effect of oblique fin arrangement by experiments and simulations, of which louvered arrangement showed better performance than inline and incline arrangement. Xu [36, 37] optimized cold plate splitter structure parameters by experiments and numerical simulations, improving the thermal equilibrium of battery pack.

The roughed elements achieved good results in the liquid cooling BTMS, but little research has been focused on the implementation of roughed elements inside the mini-channel cold plate which is expected to achieve better heat transfer performance. In this research, a new BTMS is proposed by introducing a mini-channel cold plate with circular pin fins, which have already been proved to have excellent performance in our previous work, into the BTMS for heat transfer performance enhancement. The continuously arranged pin fins are expected to re-initialize the boundary layer and transform the laminar flow into turbulent flow, resulting in better heat transfer performance and a more uniform temperature distribution. Three-dimensional (3D) numerical computations were conducted to fully characterize the fluid flow and heat transfer properties of BTMS with circular pin fins. The BTMS with circular pin fins was compared with the one without pin fins in terms of heat transfer performance and pressure loss. The effects of arrangement and layout direction of pin fins on performance of BTMS were also analyzed.

2 Numerical model

2.1 The geometry

In practice, multiple batteries are electrically connected to form battery packs to deliver required power output. In this study, a typical battery pack with 5 batteries is employed for evaluating the BTMS. Each single battery is sandwiched by two mini-channel cold plates, as illustrated in Fig.1 (a). In this research, a commercial Li-ion battery (LIB) from a battery company in Shanghai is chosen. The LIB is rectangular-shaped. The length and width of LIB are 128 mm and 79 mm respectively with a height of 12mm. The anode and cathode materials are $LiFePO_4$ and graphite, respectively. The electrolyte is the mixture of EC, DMC and EMC. The current taps are made of Al and Cu respectively with the size of 10mm length, 9mm width, and 4mm height. The specification of the battery is shown in Table 1 (a), and the thermophysical properties of LIB which were measured by high-precision hot wire thermal conductivity instrument and a calorimetric barrel are shown in the Table 1(b).

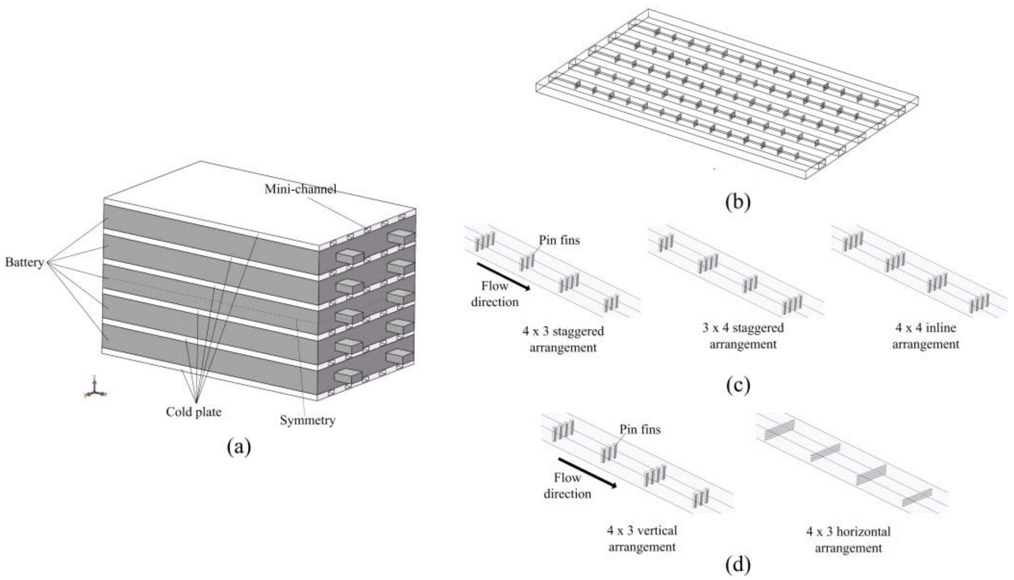

Fig.1 Schematic diagram of the battery pack (a), mini-channel cold plate (b), pin fins arrangement (c) and pin fins layout direction (d)

Table 1(a) Specifications of LIB

Contents	Battery
Normal voltage (V)	3.2
Capacity (Ah)	24
Mass (g)	400

Table 1(b) Thermophysical properties of LIB, cold plate and cooling medium

Content	Battery	Cold plate	Cooling medium
Density(kg/m^3)	1969.59	2719	998.2
Specific heat(J/kg•K)	1305	871	4182
Thermal conductivity (W/m•K)	$\lambda_x = \lambda_y = 23.7$ $\lambda_z = 3.6$	202.4	0.6
Viscosity(kg/m•s)	N/A	N/A	0.001003

Fig.1 (b) shows the mini-channel cold plates with circular pin fins. The length and width of cold plate are the same as the LIB, with a height of 3mm. According to Qian's research [29], 5 mini-channels are sufficient to achieve both better heat transfer performance and lower pressure loss. The mini-channels are uniformly distributed in the cold plate with a size of 128mm length, 5mm width, and 2mm height. All the cold plates and pin fins are made of Al, and water is chosen as the cooling medium. The thermophysical properties of the cold plate and cooling medium are also listed in Table 1.

In this research, the circular pin fins are arranged inside the straight mini-channels with an aim to enhance heat transfer by disrupting laminar boundary layer and transforming laminar flow into turbulent flow by enhancing the disturbance of the coolant. The circular pin fin has a diameter of 0.5mm and a height of 2mm. Streamwise and spanwise spacings between the centers of neighboring pin fins are 8mm and 1mm respectively. The pin fins are arranged in 14 rows. The distance between the inlet and the first row is 12mm, and the distance between outlet and the last row is also 12mm.

2.2 Mathematical model

2.2.1 Battery heating model

During charging and discharging, batteries generate a lot of heat. The temperature of batteries can be calculated by the energy conservation equation as follow [29]:

$$\rho c_p \frac{\partial T}{\partial \tau} = \frac{\partial}{\partial x}(\lambda_x \frac{\partial T}{\partial x}) + \frac{\partial}{\partial y}(\lambda_y \frac{\partial T}{\partial y}) + \frac{\partial}{\partial z}(\lambda_z \frac{\partial T}{\partial z}) + Q_g \tag{1}$$

where ρ (kg/m^3) and c_p (J/kg•K) are the battery density and specific heat capacity respectively; λ_x, λ_y, and λ_z (W/m•K) represent the heat conductivity coefficient in X, Y, and Z direction; Q_g (W) is the total generated heat, and divided into reaction heat (Q_r), ohmic heat (Q_j), and polarization heat (Q_p):

$$Q_g = Q_r + Q_j + Q_p \tag{2}$$

The reaction heat (Q_r) is generated during charging and discharging processes. It can be calculated as:

$$Q_r = -IT_b \frac{dE_{oc}}{dT_b} \tag{3}$$

Where I is discharge current, E_{oc} is the open circuit voltage, T_b is the battery temperature.

The ohmic heat (Q_j) caused by the flow of electron and ions can be determined as:

$$Q_j = I^2 R_e \tag{4}$$

Where R_e (Ω) is the ohmic resistance of the battery due to electron/ion transport.

The polarization heat (Q_p) is caused by the polarization resistance, which represents the voltage loss associated with the electrochemical processes. The polarization resistance can be determined as the difference between the total resistance and the ohmic resistance.

$$Q_p = I^2 R_p = I^2 (R_t - R_e) \tag{5}$$

Where R_p represents polarization resistance, R_t stands for the total resistance.

2.2.2 Mini-channel cold plate theoretical model

Water is the cooling medium in the proposed BTMS. The energy conservation equation of cooling medium and mini-channel cold plate can be described as follow [29]:

$$\rho_c \frac{\partial T_c}{\partial t} + \nabla\left(\rho_c \vec{v} T_c\right) = \nabla\left(\frac{\lambda_c}{c_c} \nabla T_c\right) \tag{6}$$

$$\rho_m \frac{\partial T_m}{\partial t} = \nabla\left(\frac{\lambda_m}{c_m} \nabla T_m\right) \tag{7}$$

Where ρ_c, T_c, c_c, and λ_c represents density, temperature, heat capacity, and thermal conductivity of the cooling medium respectively; $\vec{v}$ is the velocity vector of cooling medium; ρ_m, T_m, c_m, and λ_m represents density, temperature, heat capacity, and thermal conductivity of the mini-channel cold plate respectively.

The continuity and momentum conservation equations of the cooling medium are as follows [29]:

$$\frac{\partial \rho_c}{\partial t} + \nabla\left(\rho_c \vec{v}\right) = 0 \tag{8}$$

$$\frac{\partial}{\partial t}\left(\rho_c \vec{v}\right) + \nabla\left(\rho_c \vec{v}\,\vec{v}\right) + \nabla^2\left(\mu \vec{v}\right) = -\nabla P \tag{9}$$

Where P represents static pressure.

2.2.3 Parameter definition

With the installation of circular pin fins and changes of pin fins arrangements, it can be easily found that the efficient heat exchange area and available volume of the mini-channels are variable, which have a huge effect on the cooling performance and pressure loss. Therefore, the hydraulic diameter of the mini-channel is adopted to form a basis for comparing the performance of the BTMS. The hydraulic diameter of the mini-channel is defined as:

$$D_h = \frac{4\left(V_t - V_p\right)}{A_f} \tag{10}$$

Where V_t presents the volume of mini-channel without pin fins, V_p presents the volume of the pin fins, A_f is the effective heat transfer area of mini-channel.

The Reynolds number is defined as :

$$Re = \frac{\rho\, u\, L}{\mu} \tag{11}$$

Where u is the inlet velocity, and L is the hydraulic diameter of the inlet.

The overall averaged Nusselt number of the battery pack is defined as:

$$\overline{Nu}= \frac{qD_h}{\lambda_c(T_{ave} - T_c)} \tag{12}$$

Where q presents the heat flux, T_{ave} is the average temperature of the battery pack, T_c is the inlet coolant temperature, λ_c is the coolant thermal conductivity.

In liquid cooling BTMS, the implementation of roughed elements can enhance the cooling performance by re-initializing boundary layer and transforming the laminar flow into turbulent flow, but it could also be penalized by the pressure loss in the system which must be considered. The pressure loss characteristics could be represented by the friction factor f:

$$f = \frac{2\triangle PD_h}{\rho u_I^2 L_1} \tag{13}$$

Where ΔP is the pressure loss between the inlet and outlet, L_1 is the length of the mini-channel..

In the study of cooling performance of BTMS, the efficiency index, *EI*, is calculated for each CFD result to identify the optimal heat transfer design. *EI* is an overall evaluation of cooling performance considering both heat transfer and flow resistance [38]:

$$EI = \frac{\overline{Nu}/\overline{Nu_0}}{(f/f_0)^{1/3}} \tag{14}$$

Where $\overline{Nu_0}$ and f_0 are the Nusselt number and friction factor of the cold plate without pin fins, $\overline{Nu}/\overline{Nu_0}$ and f/f_0 are the normalized Nusselt number and friction factor.

2.3 Numerical methods and boundary condition

The governing equations were solved using commercial ANSYS Fluent 19.0. The flowing model used in each simulation was depending on the Reynolds number. The laminar model was selected when *Re* was less than 2300. Otherwise, the standard k-ε model was employed due to the better accuracy and computational cost as compared to the other turbulent models, which had been proved in the previous work and verified by the literature data [37]. The present study also employed a pressure-velocity coupled solver and the second-order upwind volume discretization scheme to reduce the numerical errors when analyzing the momentum and energy equations and calculating the turbulence quantities. The continuity equation as well as the velocity and turbulence quantity equations were computed till a minimum convergence value of 10^{-6} was reached.

In the numerical simulation, the following assumptions were applied to simplify the model: (1) the coolant was the incompressible fluid; (2) the heat was generated evenly; (3) the taps did not generate heat during the discharge process. The mass flow inlet boundary condition with a temperature of 303K was used for the inlet. The outlet was specified as a pressure outlet boundary condition with a value of standard atmospheric pressure. In order to reduce the computational cost, the symmetry boundary was used. The side surface of the battery pack was considered as the free convection boundary condition, and the heat transfer coefficient was defined as 5 W/(m•K). C-rate is current at which the battery is charged and discharged. In the paper the discharge rate of LIB was assumed at 9C rate with an aim to obtain the effect of pin fins under the high current discharge. The heat source was defined by UDF (user defined function) which had considered the reaction heat, ohmic heat and polarization heat to provide the accurate heat generation rate and obtain the reliable results. In addition, the no-slip boundary was also applied in mini-channel cold plate.

2.4 Mesh generation and independence verification

A structured hexahedral mesh was generated for all the computation cases using ICEM commercial mesh generation software. The cell orthogonally was ensured by the introduction of multiple O-gird type blocks for all circular pin fins, and the mesh quality of all the models was bigger than 0.8. The y+ value of all the models in the investigation is lower than 1, and the y+ value is a dimensionless parameter for the distance away from the wall. Grid independence check was performed for each computation grid system with the mesh numbers ranging from about 2.5 million to 12.6 million, as shown in Fig.2 (a). With the increase in the total grid number, the computation results became to be invariable and the changes in temperature and pressure loss. Considering the quality of grids, numerical accuracy, and computational time, a mesh number of about 8.4 million was chosen for all the computations, as shown in Fig.2 (b).

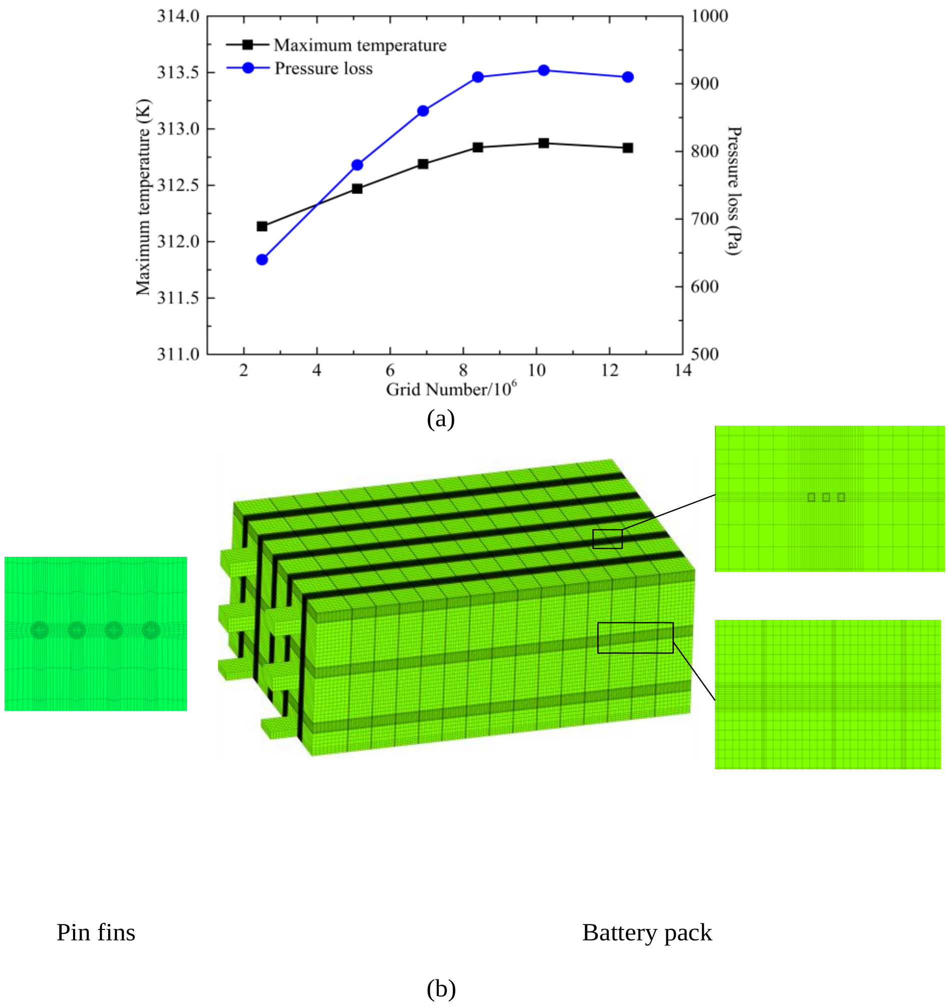

Fig.2 Grid independence study results (a), and schematic mesh of the calculation model (b)

3 Results and discussion

3.1 Model validation

In order to verify the accuracy of the numerical model used in the simulations, a comparison between the present maximum temperature and the data by Qian [29] and Rao [39] was performed. Fig.3 shows the maximum temperature of battery pack with no battery thermal management system when the discharge rate was chosen as 5C. The data deviations on maximum temperature were less than 0.38K and 0.52K respectively, which were considered acceptable. The good agreement between the numerical results and the data from the literature well validate the model for subsequent parametric simulation and optimal design.

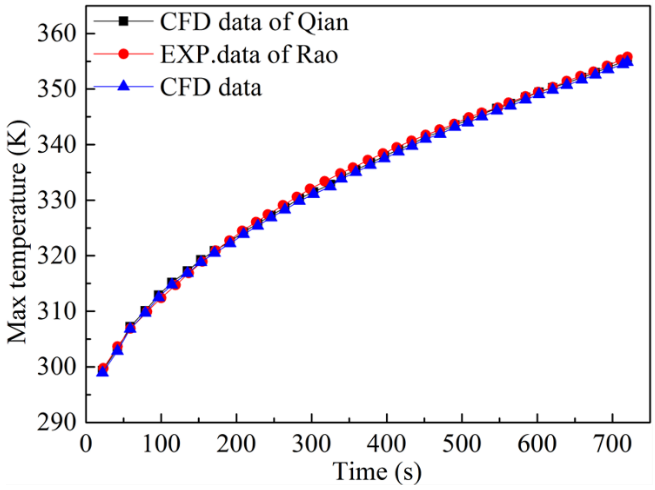

Fig.3 Comparison of numerical result with published numerical and experimental results

3.2 The effect of pin fins

In order to investigate the effect of circular pin fins on the cooling performance of BTMS, numerical simulations were conducted under different mass flow rates to obtain the maximum temperature and maximum temperature difference of battery pack, the maximum temperature difference of single battery, and average heat flux of mini-channels. Fig.4 (a) shows the maximum temperature of the battery pack under different mass flow rates at the end of 9C discharge. It can be seen that the maximum temperature decreased with the increasing mass flow rate. The pin fins arranged BTMS always achieved better cooling performance, and the maximum temperature was 1.32K, 1.71K, 1.85K, 1.89K, and 1.9K lower respectively than BTMS without any pin fins. In addition, the maximum temperature of the battery pack without pin fins could only be cooled down to below 313K at a high mass flow rate of 0.005 kg/s. For comparison, only 0.003 kg/s was needed for the battery pack with circular pin fins to reach this temperature.

The maximum temperature differences of single battery and battery pack decreased as the mass flow rate increases, as shown in Fig.4 (b) and Fig.4 (c). Under the investigated mass flow rates, the max temperature difference within the single battery could be reduced by 0.88K, 1.37K, 1.58K, 1.69K, and 1.75K due to the implementation of circular pin fins, and maximum temperature difference within the battery pack was decreased by 1.01K, 1.51K, 1.71K, 1.8K, and 1.85K after arranging circular pin fins. Besides, 0.003 kg/s and 0.005 kg/s mass flow rates are needed to control the maximum temperature difference between single battery and battery pack within 5K when pin fins arranged BTMS was used, but BTMS without pin fins never reached this temperature difference under the investigated mass flow rates.

The average heat flux of mini-channels shown in Fig.4 (d) reveals why pin fins arranged BTMS have a favorable heat transfer performance and temperature distribution. With circular pin fins, the average heat flux is increased by 7.14%, 8.63%, 9.4%, 9.82%, and 10.12% as compared to the BTMS without pin fins. This is because that pin fins not only increase heat exchange areas but also refresh the boundary layer development and transform the laminar flow into turbulent flow by enhancing the disturbance of coolant, as shown in Fig.4 (e). It can be distinctly observed that a lot of swirling vortexes are generated after coolant flowing through the pin fins.

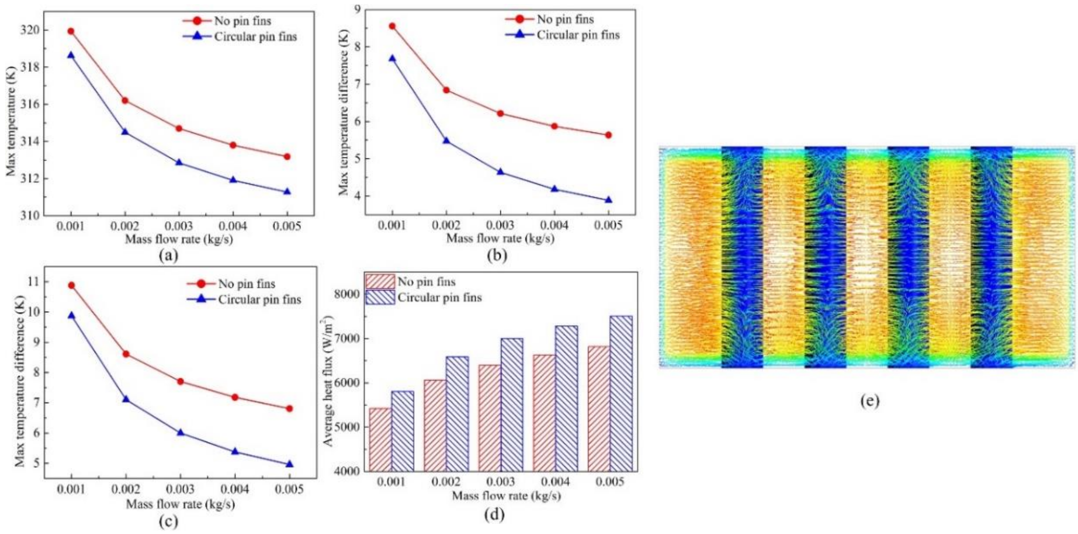

Fig.4 Maximum temperature (a), maximum temperature difference within single battery (b), maximum temperature difference within battery pack (c), average heat flux of mini-channel (d) under different mass flow rates, and 3D streamlines of coolant after flowing through pin

fins (e)

Fig.5 depicts the temperature distribution of the battery pack under different mass flow rates. Increasing mass flow rate can help achieve a better temperature distribution of the battery pack for both designs. For all the cases, the minimum temperature of every single battery always appeared around the coolant inlet, and then the temperature increased along the flow direction due to heat generation from the battery. Besides, lower temperature also appeared at the electrode surface and near-electrode surface as compared to the battery, as the heat can be more effectively taken away from the electrode surface. It is important to note that the battery pack with pin fins arranged BTMS showed a smaller temperature gradient, indicating a more uniform temperature distribution within the battery pack and every single battery. The highest temperature of every single battery appeared around the intermediate area, and the maximum temperature of battery pack appeared at the central section of cell 3, as presented in Fig.6. At a low coolant flow rate, the central section of each battery showed higher temperature due to the insufficient cooling effect of BTMS. With increasing coolant flow rate, the heat generated from the batteries could be effectively removed, which decreased the maximum temperature in the battery and improved the temperature uniformity.

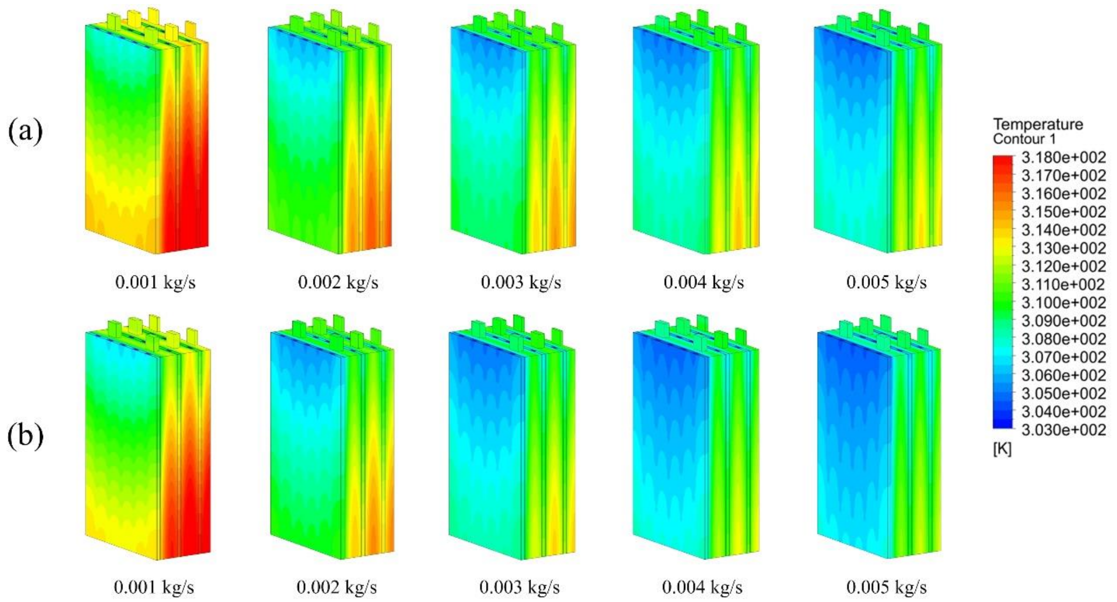

Fig.5 Temperature distribution under different mass flow rates.

(a) no pin fins (b) circular pin fins

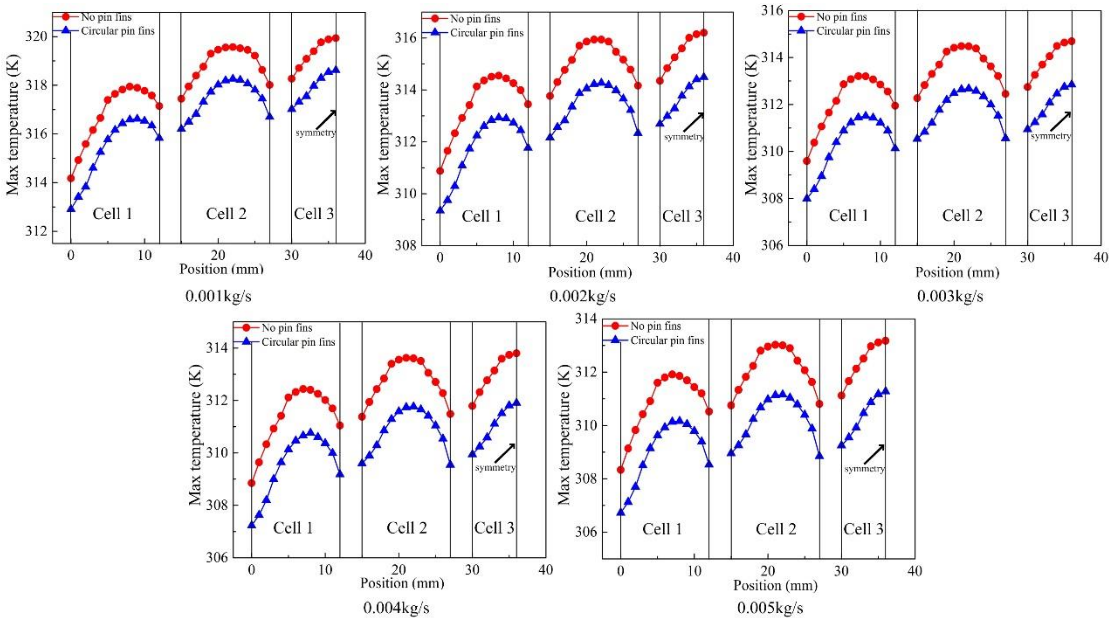

Fig.6 Max temperature distribution along Z-direction under different mass flow rate

In liquid cooling BTMS, the heat transfer enhancement caused by pin fins could be penalized by the adverse effect of pressure loss. Thus, pressure loss is another critical factor in the evaluation of the BTMS. Hence, the optimal goal of the BTMS design is to achieve better heat transfer with acceptable pressure loss. Table 2 shows the pressure drop and normalized friction factor of the BTMS with and without circular pin fins, respectively. All values of normalized friction factor of the BTMS with pin fins exceeded 1, which implied that pin fins would increase the extra friction factor in the BTMS. Under the investigated mass flow rates, the pin fins arranged BTMS always caused higher pressure loss than BTMS without pin fins by 82.5 Pa, 187.06 Pa, 314.25 Pa, 462.71 Pa, and 632.23 Pa, respectively.

Table 2 Pressure drop and normalized friction factor of two structures

Mass flow rate (kg/s)	Pressure drop (Pa)		Normalized friction factor	
	No pin fins	Circular pin fins	No pin fins	Circular pin fins
0.001	178.37	260.81	N/A	1.26
0.002	378.69	565.75	N/A	1.29

0.003	596.9	911.15	N/A	1.32
0.004	833.18	1295.89	N/A	1.35
0.005	1086.23	1718.46	N/A	1.37

Fig.7 presents the 3D streamlines and local temperature distribution for the mini-channel with circular pin fins under different mass flow rates, which strongly indicate the fluid flow and heat transfer. The impingement of coolant on the surface of pin fins could refresh the boundary layer development, transform the laminar flow into the turbulent flow and enhance the heat transfer along the surface of the pin fins. The coolant flowing between the pin fins accelerated significantly due to the narrower channels caused by the pin fins. Then the coolant impinging on the pin fins and flow between pin fins would be mixed in the downstream, promoting 3D turbulent mixing, re-initializing the boundary layer and improving the heat transfer performance of the other areas of mini-channels except for the areas around pin fins. Therefore, a high heat transfer region could always be observed around the pin fins regardless of mass flow rates. Within the studied flow rate range, the coolant still contacted with the surface of pin fins in the downstream area, and there were no apparent phenomena of flow separation and vortex shedding during the coolant flow through the pin fins. Therefore, the increase in the pressure loss and friction factor caused by circular pin fins were controlled in a reasonable range. However, the velocity of the coolant behind the pin fins was relatively low, which could cause a local low heat transfer rate.

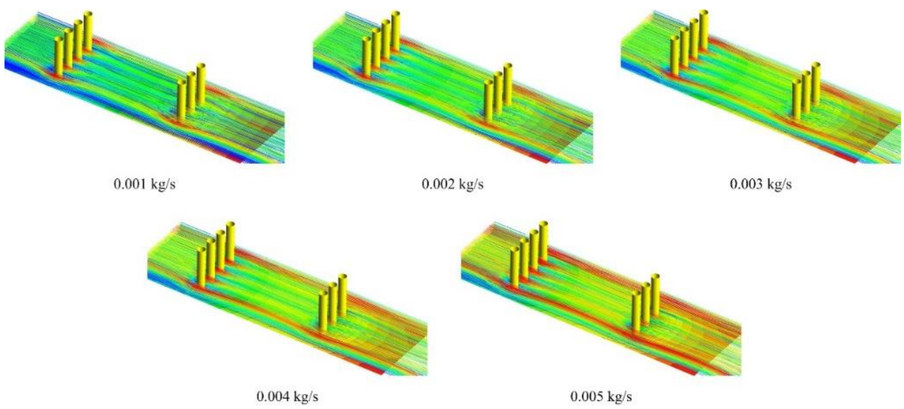

Fig.7 3D streamlines and temperature distribution under different mass flow rate

To further evaluate the cooling performance of the BTMS with circular pin fins, the efficiency index (*EI*) was calculated for each result obtained in this study. Higher *EI* implies more favorable overall cooling performance with high heat transfer performance and acceptable pressure loss. Fig.8 depicts the *EI* of BTMS with circular pin fins under different mass flow rates. It can be observed that all cases exhibited *EI* greater than 1, indicating that the implementation of pin fins enhanced heat transfer with acceptable friction factor increment. It means that circular pin fins could enhance the overall cooling performance of the BTMS. It is also observed that the *EI* value increased with increasing mass flow rate. However, the increment in *EI* became smaller when the flow rate was further increased beyond 0.003 kg/s. Therefore, the mass flow rate in BTMS is not necessary to be very high in practical applications. Considering the maximum temperature, maximum temperature difference, pressure drop and efficiency index, a coolant mass flow rate of 0.003 kg/s is enough for the battery pack to meet the requirements of working temperature when operating at 9C rate. So, in the following research, simulations were conducted at a mass flow rate of 0.003 kg/s.

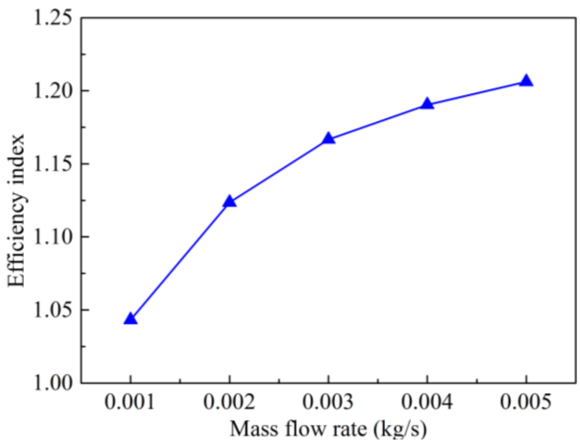

Fig.8 Efficiency index under different mass flow rate

3.3 The effect of pin fins arrangement

For heat transfer enhancement, inline arrangement and staggered arrangement of pin fins are commonly used for heat transfer engineering design. Even with a given number of pin fins, different pin fins arrangements can still induce different flow structures, resulting in different heat transfer behaviors and friction factors. However, such study has not been reported for BTMS yet. Therefore, in order to investigate the effect of pin fins arrangement and choose the best pin fins arrangement for BTMS with mini-channel cold plate, one inline scheme and two different staggered schemes were developed, as shown in Fig.1(c).

Fig.9 (a), Fig.9 (b), and Fig.9 (c) present the maximum temperature of the battery pack, maximum temperature difference within the single battery, and maximum temperature difference within the battery pack, respectively. It can be observed that all three parameters were varied as time passing, and the changing trend also had big differences in the different discharge states. In the early state of discharging, the amount of heat generated by battery was increased rapidly. However, as the temperature of battery is close to that of the BTMS and the surrounding environment at the beginning, the rate of heat transfer from the battery to the coolant is small due to small temperature difference. As the amount of generated heat is increased with time, the maximum temperature and temperature difference of both single battery and battery pack increased rapidly. On the other hand, with increasing temperature and the temperature difference, the heat transfer from the battery to the coolant is also enhanced due to the increased driving force (temperature difference) for heat transfer, which would limit the temperature rise of the battery. However, the mass transfer polarization effect increased rapidly at the end of discharging, leading to a sharply increased battery total internal resistance and heat generation rate. Therefore, the maximum temperature and maximum temperature difference were found to increase substantially at the end of discharge. During the whole period of discharging, battery pack with 4 x 4 inline arranged pin fins always achieved the lowest maximum temperature and temperature difference, but the difference between these three pin fins arrangement was very small. As compared to the BTMS with no pin fins, 4 x 3 staggered arranged pin fins and 3 x 4 staggered arranged pin fins, the maximum temperature was lowered by 2.16K, 0.32K and 0.29K, the maximum temperature within the single battery was lowered by 1.82K, 0.24K and 0.17K, the maximum temperature within battery pack was lowered by 1.97K, 0.27K and 0.21. Fig.9 (d) presents the average heat flux of mini-channels. It can be found that BTMS without pin fins showed the lowest average heat flux, and the BTMS with 4 x 4 inline arranged pin fins show the highest average heat flux.

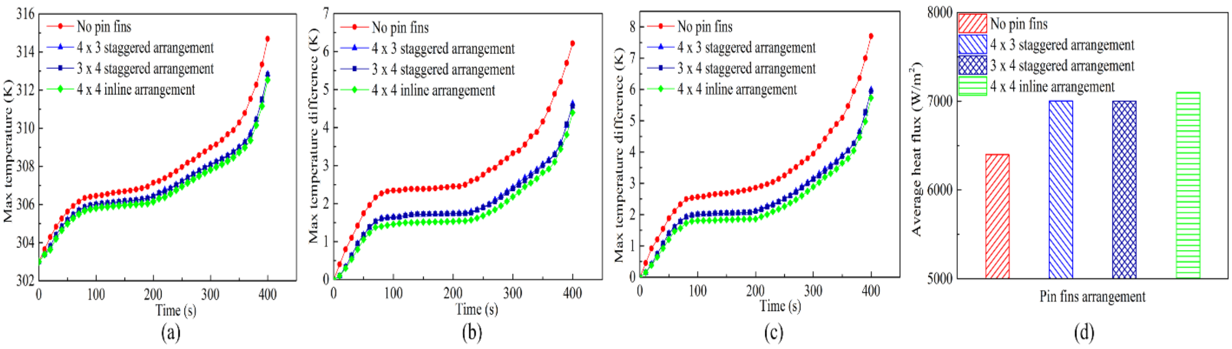

Fig.9 Maximum temperature (a), maximum temperature difference within single battery (b), maximum temperature difference within battery pack (c) and average heat flux of mini-channel (d) for different pin fins arrangement

Fig.10 (a) depicts the temperature distribution of the battery pack with differently arranged pin fins and without pin fins. It can be observed that the battery pack with BTMS arranged by all these three pin fins arrangements showed smaller temperature gradient, indicating that a more uniform temperature distribution within the battery pack and every single battery could be achieved in these three cases. However, the temperature distribution in these three cases was very similar to each other. Fig.10 (b) presents the maximum temperature distribution along Z-direction. All the cases had the similar trend: the temperature around the intermediate area was always higher than the temperature in the two sides in every single battery and the maximum temperature of the battery pack appeared at the central section of cell 3. In addition, BTMS with 4 x 4 inline arranged pin fins always achieved lower maximum temperature along Z-direction than that of BTMS with 4 x 3 staggered and 3 x 4 staggered arranged pin fins.

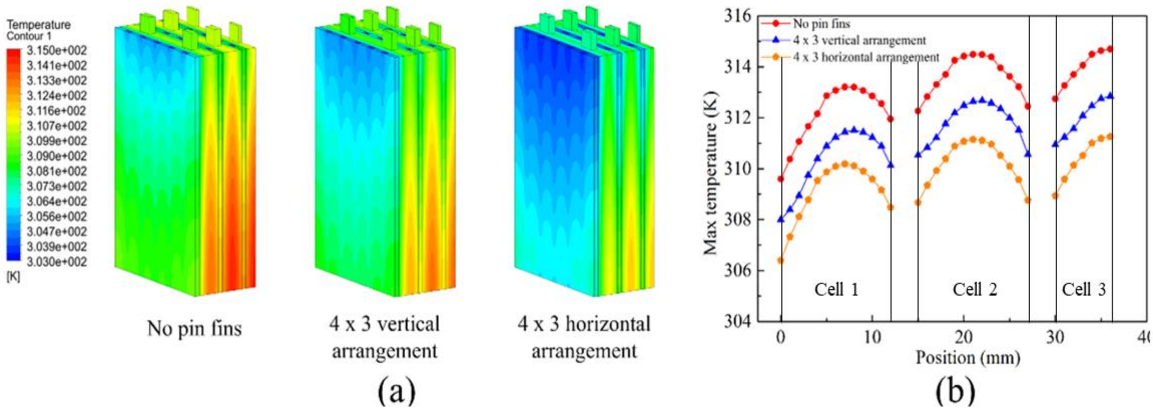

Fig.10 Temperature distribution (a), and max temperature distribution along Z-direction rake (b) for different pin fins arrangement

Table 3 shows the pressure drop and normalized friction factor of the BTMS with differently arranged pin fins. As compared to the BTMS without pin fins, the BTMS arranged with pin fins by using these three arrangements always cause higher pressure loss and friction factor. In addition, the extra pressure loss and friction factor caused by 4 x 3 staggered and 3 x 4 staggered arranged pin fins were very similar. The BTMS with 4 x 4 inline arranged pin fins had the highest pressure drop and normalized friction factor. Its pressure drop was 197.8 Pa and 193.4 Pa higher than that of 4 x 3 staggered and 3 x 4 staggered arranged pin fins, respectively. Its normalized friction factor was 0.254 and 0.252 higher than 4 x 3 staggered and 3 x 4 staggered arranged pin fins, respectively.

Table 3 Pressure drop and normalized friction factor of different pin fins arrangements

Pin fins arrangement	No pin fins	4 x 3 staggered arrangement	3 x 4 staggered arrangement	4 x 4 inline arrangement
Pressure drop (Pa)	596.9	911.15	915.61	1108.97
Normalized friction factor	None	1.323	1.325	1.577

Fig.11 presents the 3D streamlines and local temperature distribution for the mini-channel with differently arranged pin fins, indicating why 4 x 3 staggered, 3 x 4 staggered and 4 x 4 inline arranged pin fins could result in different heat transfer performance and pressure loss. Firstly, the coolant showed the similar flow structure when the coolant passed through the pin fins in all these three cases. As the coolant flowing downstream, a part of the coolant would impact the surface of pin fins, and then flowed between pin fins and wall or between pin fins. Therefore, the coolant velocity would be increased, the boundary layer would be re-initialized, and 3D turbulent mixing could be generated. However, the mass flow rate used in all these cases was just 0.003 kg/s. Thus, the disturbance of coolant began to decrease, and the thickness of the boundary layer started to increase before the coolant reaching the next row of pin fins. At this time, the coolant almost returned to laminar flow. Hence, the pin fins had less effect on coolant flowing structure around the other row of pin fins, even two adjacent rows of pin fins. Therefore, due to the more compact arranged pin fins compared to the 4 x 3 staggered and 3 x 4 staggered arranged pin fins, 4 x 4 inline arranged pin fins can be more helpful in improving heat transfer performance but also lead to a higher pressure drop.

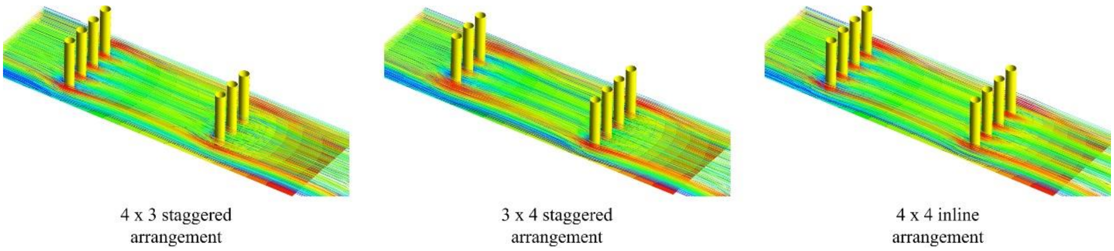

Fig.11 3D streamlines and temperature distribution for three pin fins arrangement

Table 4 presents the *EI* of BTMS with different arranged circular pin fins. The BTMS with two staggered arranged pin fins had a similar *EI*. The BTMS with 4 x 3 staggered arranged pin fins showed the highest *EI*, which was attributed to the effect of favorable heat transfer performance and friction factor. The BTMS with 4 x 4 inline arranged pin fins achieved the best heat transfer performance with the biggest pressure loss, leading to the lowest *EI*. Considering the trade-offs between heat transfer and friction factor in the design of the pin fins arrangement, the 4 x 3 staggered arrangement can be the best option.

Table 4 Efficiency index for three pin fins arrangements

Pin fins arrangement	4 x 3 staggered arrangement	3 x 4 staggered arrangement	4 x 4 inline arrangement
Efficiency index (*EI*)	1.167	1.165	1.156

3.4 The effect of pin fins layout direction

The flow structures are distinctly different in the mini-channels with different pin fin layout directions, leading to the totally different heat transfer performance and friction factor. Thus, in order to evaluate the influence of pin fins layout direction on heat transfer performance, flow resistance and efficiency index, 4 x 3 vertical arrangement and 4 x 3 horizontal arrangement of pin fins with the similar hydraulic diameter of the mini-channel were investigated. The schematic was shown in Fig.1(d).

Fig.12 (a), Fig.12 (b), and Fig.12 (c) present the maximum temperature of the battery pack, maximum temperature difference within the single battery, and maximum temperature difference within the battery pack, respectively. The BTMS with horizontally arranged pin fins achieved the lowest maximum temperature of the battery pack, which was 3.43K and 1.59K lower than that of BTMS with no pin fins and vertically arranged pin fins. However, the maximum temperature difference within the single battery and battery pack of BTMS with horizontally arranged pin fins were lower than that of BTMS without pin fins by 0.56K and 1.22K, but higher than that of BTMS with 4 x 3 vertically arranged pin fins by 1.03K and 0.49K. Fig.12 (d) presents the average heat flux of mini-channels. It is shown that there was a big difference in average heat flux for these three cases. The BTMS with horizontally arranged pin fins showed the highest average heat flux, which was 20.56% and 10.23% higher than that of BTMS with no pin fins and vertically arranged pin fins.

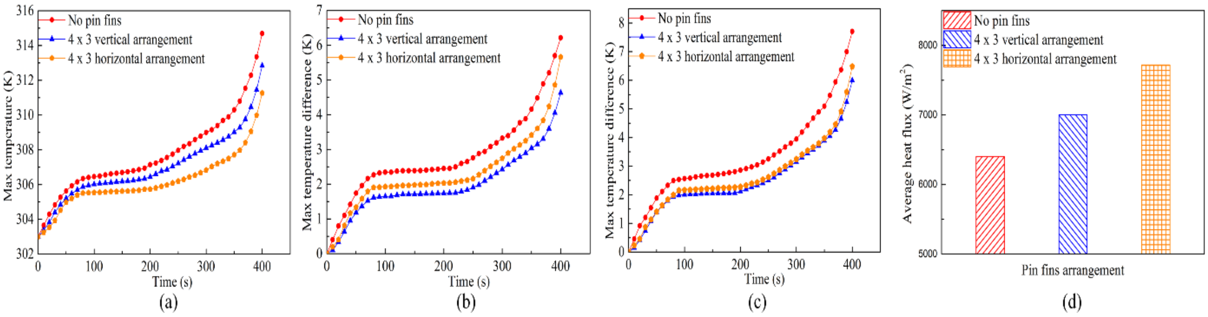

Fig.12 Maximum temperature (a), maximum temperature difference within single battery (b), maximum temperature difference within battery pack (c) and average heat flux of mini-channel (d) for different pin fins arrangement

Fig.13 (a) shows the temperature distribution of the battery pack with differently arranged pin fins and no pin fins. The temperature distribution of these three cases is very different from each other. The BTMS with horizontally arranged pin fins could achieve the best cooling performance, and the cell 2 and cell 3 had the similar temperature distribution in this case. However, the temperature gradient was only smaller than that of BTMS with no pin fins but higher than that of BTMS with vertically arranged pin fins. Fig.13 (b) presents the maximum temperature distribution along Z-direction. The temperature distributions of the 3 battery packs were similar while the BTMS with 4x3 horizontal pin fin arrangement showed the lowest temperature among the 3 cases.

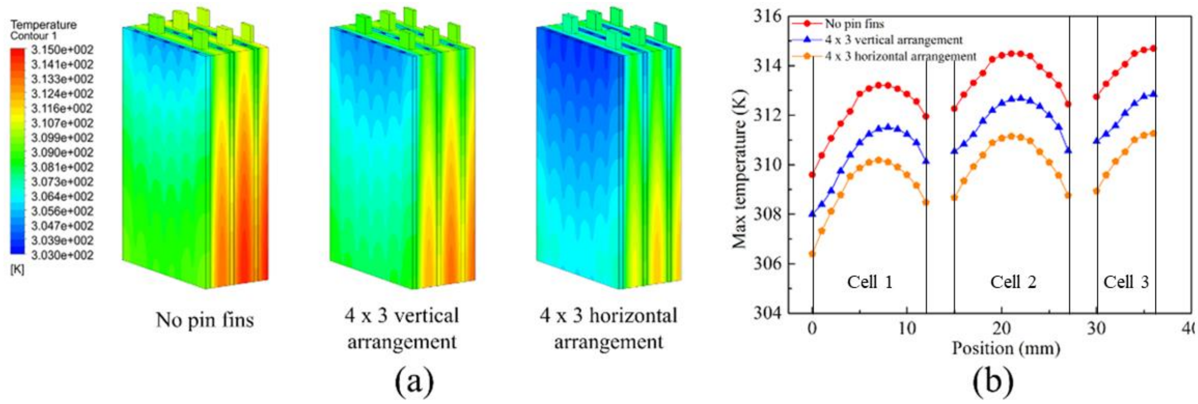

Fig.13 Temperature distribution (a), and max temperature distribution along Z-direction rake (b) for different pin fins arrangement

Table 5 shows the pressure drop and normalized friction factor, respectively. The pressure loss caused by horizontal pin fins arranged BTMS was much higher than BTMS with no pin fins and vertically arranged pin fins by almost 8 times and 4 times, respectively. The normalized friction factor of horizontal pin fins arranged BTMS was almost 2.5 times bigger than that of BTMS with vertically arranged pin fins.

Table 5 Pressure drop and normalized friction factor of different pin fins arrangements

Pin fins arrangement	No pin fins	4 x 3 vertical arrangement	4 x 3 horizontal arrangement
Pressure drop (Pa)	596.9	911.15	4530.94
Normalized friction factor	None	1.323	3.278

The 3D streamlines and local temperature distribution are shown in Fig.14 to understand why horizontally arranged pin fins produced distinctly different heat transfer performance and pressure loss with vertically arranged pin fins. As we can see, all the mini-channels had the small height. Therefore, there was a strong interaction between the coolants as the coolant passing through the pin fins which were horizontally arranged inside BTMS, leading to the intense turbulence. It can be clearly seen that the large-scale vortex was generated in the mini-channel due to the horizontally arranged pin fins. Especially at the top and bottom of the mini-channel, the flow velocities and the intensity of the turbulence were very high. In addition, the cooling fluid could maintain the high velocity and turbulence as it flows downstream, and the velocity and turbulence would be higher during this period. Therefore, horizontally arranged pin fins achieved the best heat transfer performance but were penalized with the adverse effect of high pressure loss.

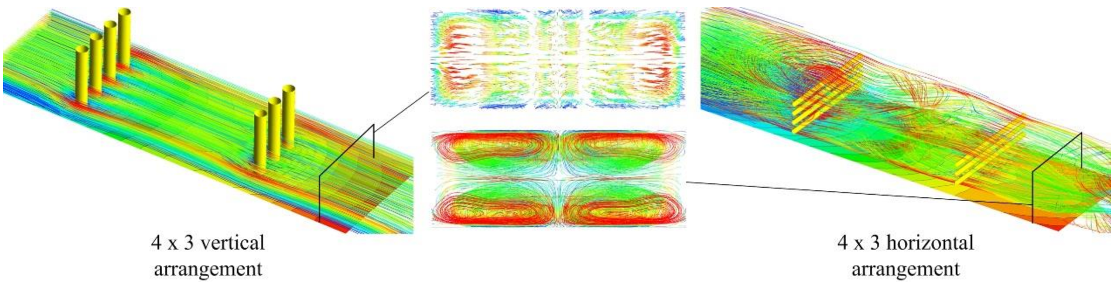

Fig.14 3D streamlines and temperature distribution for two pin fins arrangement

Table 6 shows the *EI* of BTMS with differently arranged pin fins. It is noted that the *EI* of the BTMS with vertically arranged pin fins was higher than that of the BTMS with horizontally arranged pin fins. Although the BTMS with horizontally arranged pin fins achieved much higher heat transfer enhancement than the BTMS with vertically arranged pin fins, it also suffered from significantly higher pressure loss. Considering the heat transfer and friction factor, the 4 x 3 vertical arrangement can be the best choice.

Table 6 Efficiency index of different pin fins arrangements

Pin fins arrangement	4 x 3 vertical arrangement	4 x 3 horizontal arrangement
Efficiency index (*EI*)	1.167	1.114

4 Conclusions

In order to control the undesirable thermal performance of the battery pack operating at the high current, a new type of BTMS with circular pin fins was introduced in this paper. The effects of circular pin fins, pin fins arrangement and pin fins layout direction on the temperature, temperature distribution, pressure drop, and flow structure of battery pack were systematically studied. The conclusions are summarized below:

(1) The pin fins arranged BTMS achieved better cooling performance. Due to the implementation of circular pin fins, the maximum temperature was reduced by 1.32K, 1.71K, 1.85K, 1.89K, and 1.9K, the maximum temperature difference within single battery could be reduced by 0.88K, 1.37K, 1.58K, 1.69K, and 1.75K, and maximum temperature difference within the battery pack was decreased by 1.01K, 1.51K, 1.71K, 1.8K, and 1.85K.

(2) BTMS with circular pin fins exhibited *EI* greater than 1, indicating enhanced heat transfer with acceptable friction factor increase. The *EI* was found to increase with

increasing mass flow rate and the increment was smaller at a high flow rate.

(3) 4 x 4 inline pin fins arranged BTMS had a better thermal behavior with a higher pressure loss as compared to the BTMS with 4 x 3 staggered and 3 x 4 staggered pin fins. However, 4 x 3 staggered arranged pin fins could be the best choice among these pin fins arrangements as referring to the efficiency index.

(4) A much higher heat transfer enhancement and more significant pressure loss was achieved by horizontally arranged pin fins as compared to the vertically arranged pin fins. However, BTMS with horizontally arranged pin fins achieved the bad *EI*, which was lower than that of BTMS with vertically arranged pin fins by 4.54%

Data Availability:

The data presented in the paper can be available upon request from the first author, Mr. Zengjia Guo (guozengjia.guo@connect.polyu.hk).

Acknowledgement:

This research is supported by a grant under the Theme-based Scheme (project number: T23-601/17-R) from Research Grant Council, University Grants Committee, Hong Kong SAR.

References

[1] Guo G, Long B, Cheng B, et al. Three-dimensional thermal finite element modeling of lithium-ion battery in thermal abuse application. Journal of Power Sources. 2010;195:2393-8.

[2] Pesaran AA, Vlahinos A, Burch SD. Thermal performance of EV and HEV battery modules and packs. National Renewable Energy Laboratory; 1997.

[3] Khateeb SA, Amiruddin S, Farid M, et al. Thermal management of Li-ion battery with phase change material for electric scooters: experimental validation. Journal of Power Sources. 2005;142:345-53.

[4] Ishikawa H, Mendoza O, Nishikawa Y, et al. Thermal characteristics of lithium ion secondary cells in high temperature environments using an accelerating rate calorimeter. Journal of Renewable and Sustainable Energy. 2013;5:043122.

[5] Yan J, Wang Q, Li K, et al. Numerical study on the thermal performance of a composite board in battery thermal management system. Applied Thermal Engineering. 2016;106:131-40.

[6] Pesaran AA. Battery thermal models for hybrid vehicle simulations. Journal of power sources. 2002;110:377-82.

[7] Na X, Kang H, Wang T, et al. Reverse layered air flow for Li-ion battery thermal management. Applied

Thermal Engineering. 2018;143:257-62.

[8] Saw LH, Ye Y, Tay AA, et al. Computational fluid dynamic and thermal analysis of Lithium-ion battery pack with air cooling. Applied energy. 2016;177:783-92.

[9] Wang T, Tseng K, Zhao J, et al. Thermal investigation of lithium-ion battery module with different cell arrangement structures and forced air-cooling strategies. Applied energy. 2014;134:229-38.

[10] Yang N, Zhang X, Li G, et al. Assessment of the forced air-cooling performance for cylindrical lithium-ion battery packs: A comparative analysis between aligned and staggered cell arrangements. Applied thermal engineering. 2015;80:55-65.

[11] Al Hallaj S, Selman J. A novel thermal management system for electric vehicle batteries using phase - change material. Journal of the Electrochemical Society. 2000;147:3231-36.

[12] Rao Z, Wang S. A review of power battery thermal energy management. Renewable and Sustainable Energy Reviews. 2011;15:4554-71.

[13] Quanying Y, Chen L, Lin Z. Experimental study on the thermal storage performance and preparation of paraffin mixtures used in the phase change wall. Solar Energy Materials and Solar Cells. 2008;92:1526-32.

[14] Karimi G, Azizi M, Babapoor A. Experimental study of a cylindrical lithium ion battery thermal management using phase change material composites. Journal of Energy Storage. 2016;8:168-74.

[15] Samimi F, Babapoor A, Azizi M, et al. Thermal management analysis of a Li-ion battery cell using phase change material loaded with carbon fibers. Energy. 2016;96:355-71.

[16] Ye Y, Saw LH, Shi Y, et al. Numerical analyses on optimizing a heat pipe thermal management system for lithium-ion batteries during fast charging. Applied Thermal Engineering. 2015;86:281-91.

[17] Zhang Z, Wei K. Experimental and numerical study of a passive thermal management system using flat heat pipes for lithium-ion batteries. Applied Thermal Engineering. 2020;166:114660.

[18] Wang L, Zhao Y, Quan Z, et al. Investigation of thermal management of lithium-ion battery based on micro heat pipe array. Journal of Energy Storage. 2021;39:102624.

[19] Smith J, Hinterberger M, Hable P, et al. Simulative method for determining the optimal operating conditions for a cooling plate for lithium-ion battery cell modules. Journal of Power Sources. 2014;267:784-92.

[20] Chen D, Jiang J, Kim G-H, et al. Comparison of different cooling methods for lithium ion battery cells. Applied Thermal Engineering. 2016;94:846-54.

[21] Sefidan AM, Sojoudi A, Saha SC. Nanofluid-based cooling of cylindrical lithium-ion battery packs employing forced air flow. International Journal of Thermal Sciences. 2017;117:44-58.

[22] Angayarkanni S, Philip J. Effect of nanoparticles aggregation on thermal and electrical conductivities of nanofluids. Journal of Nanofluids. 2014;3:17-25.

[23] Yang X-H, Tan S-C, Liu J. Thermal management of Li-ion battery with liquid metal. Energy conversion and management. 2016;117:577-85.

[24] Panchal S, Khasow R, Dincer I, et al. Thermal design and simulation of mini-channel cold plate for water cooled large sized prismatic lithium-ion battery. Applied Thermal Engineering. 2017;122:80-90.

[25] Jarrett A, Kim IY. Influence of operating conditions on the optimum design of electric vehicle battery cooling plates. Journal of Power sources. 2014;245:644-55.

[26] Karimi G, Dehghan A. Thermal management analysis of a lithium-ion battery pack using flow network approach. International Journal of Mechanical Engineering and Mechatronics. 2012;1:88-94.

[27] Hao Y, Li-Fang W, Li-Ye W. Battery thermal management system with liquid cooling and heating in electric vehicles. Journal of Automotive Safety and Energy. 2012;3:371-80.

[28] Huo Y, Rao Z, Liu X, et al. Investigation of power battery thermal management by using mini-channel cold plate. Energy Conversion and Management. 2015;89:387-95.

[29] Qian Z, Li Y, Rao Z. Thermal performance of lithium-ion battery thermal management system by using mini-channel cooling. Energy Conversion and Management. 2016;126:622-31.

[30] Xie X, Liu Z, He Y, et al. Numerical study of laminar heat transfer and pressure drop characteristics in a water-cooled minichannel heat sink. Applied thermal engineering. 2009;29:64-74.

[31] Zhang Y, Wang S, Ding P. Effects of channel shape on the cooling performance of hybrid micro-channel and slot-jet module. International journal of heat and mass transfer. 2017;113:295-309.

[32] Lee Y-J, Lee P-S, Chou S-K. Hot spot mitigating with oblique finned microchannel heat sink. ASME International Mechanical Engineering Congress and Exposition. 2010;4:167-74.

[33] Jin L, Lee P, Kong X, et al. Ultra-thin minichannel LCP for EV battery thermal management. Applied energy. 2014;113:1786-94.

[34] Mohammed AH, Esmaeeli R, Aliniagerdroudbari H, et al. Dual-purpose cooling plate for thermal management of prismatic lithium-ion batteries during normal operation and thermal runaway. Applied Thermal Engineering. 2019;160:114106.

[35] Om NI, Zulkifli R, Gunnasegaran P. Influence of the oblique fin arrangement on the fluid flow and thermal performance of liquid cold plate. Case studies in thermal engineering. 2018;12:717-27.

[36] Fu J, Xu X, Li R. Battery module thermal management based on liquid cold plate with heat transfer enhanced fin. International Journal of Energy Research. 2019;43:4312-21.

[37] Xu X, Tong G, Li R. Numerical study and optimizing on cold plate splitter for lithium battery thermal management system. Applied Thermal Engineering. 2020;167:114787.

[38] Chi Z, Kan R, Ren J, et al. Experimental and numerical study of the anti-crossflows impingement cooling structure. International Journal of Heat and Mass Transfer. 2013;64:567-80.

[39] Rao Z, Huo Y, Liu X, et al. Experimental investigation of battery thermal management system for electric vehicle based on paraffin/copper foam. Journal of the Energy Institute. 2015;88:241-6.